



System design and measurements of flux concentrator and its solid-state modulator for CEPC positron source

Jing-Dong Liu^{1,2} · Xiao-Ping Li² · Cai Meng^{2,3} · Yun-Long Chi² · Guo-Xi Pei^{2,3} · Da-Yong He² · Jing-Yi Li² · Xian-Jing Sun² · Jing-Ru Zhang² · Lei Shang¹ · Jian-Bin Zhu^{2,3}

Received: 24 December 2020 / Revised: 19 April 2021 / Accepted: 13 May 2021 / Published online: 27 July 2021
© China Science Publishing & Media Ltd. (Science Press), Shanghai Institute of Applied Physics, the Chinese Academy of Sciences, Chinese Nuclear Society 2021

Abstract Positron sources are one of the most important components of the injector of a circular electron positron collector (CEPC). The CEPC is designed as an e^+e^- collider for a Higgs factory. Its accelerator system is composed of 100-km-long storage rings and an injector. The design goal of the positron source is to obtain positron beams with a bunch charge of 3 nC. The flux concentrator (FC) is one of the cores of the positron source. This paper reports the design, development, and measurements of an FC prototype system. The prototype includes an FC and an all-solid-state high-current pulse modulator. Preliminary tests show that the peak current on the FC can reach 15.5 kA, and the peak magnetic field can reach 6.2 T. The test results are consistent with the theoretical simulation. The FC system fulfills the requirements of the CEPC positron source as well as provides a reference for the development of similar devices both domestically and abroad.

Keywords CEPC positron source · Flux concentrator · Solid-state modulator · High current · Peak magnetic field

1 Introduction

The circular electron–positron collider (CEPC) is proposed as an electron–positron collider that resides in a 100-km-long circular tunnel and operates at a center-of-mass energy of 90–240 GeV to produce Z, W, and Higgs bosons [1–3]. The conceptual design report (CDR) [1] of the collider was published in August 2018. According to the CDR, the injector, which is a key component of the collider, comprises a 10 GeV Linac, a full energy booster, and the corresponding transport lines. The Linac is designed to provide electron and positron beams with energies of approximately 10 GeV and bunch charge up to 3 nC. The layout of the CEPC Linac is illustrated in Fig. 1. The Linac comprises a pre-injector, first acceleration section, positron source and pre-accelerating section (PSPAS), second acceleration section, and third accelerating section. The pre-injector includes an electron gun (eGun) and a bunching system (BS). The eGun produces electron beams (EBs) with bunch charges of 3 and 10 nC for colliding EBs and producing positron beams, respectively. The first accelerating section, named Linac1, was used to boost the energy of the EBs to approximately 4 GeV. At the end of Linac1, the EBs would traverse different paths depending on their usage. The colliding EB passes through an electron bypass transport line, whereas the other EB type enters the PSPAS directly. The PSPAS comprises a target, flux concentrator (FC), and pre-acceleration section [4]. In the PSPAS, positrons are generated by colliding the EBs with the target, focusing using the FC, and

This work was supported by the National Key Programme for S&T Research and Development (No. 2016YFA0400400) and the Youth Innovation Promotion Association CAS (2019016).

✉ Xiao-Ping Li
lxp@ihep.ac.cn

- ¹ National Synchrotron Radiation Laboratory, University of Science and Technology of China, Hefei 230029, China
- ² Key Laboratory of Particle Acceleration Physics and Technology, Institute of High Energy Physics, Chinese Academy of Sciences, Beijing 100049, China
- ³ University of Chinese Academy of Sciences, Beijing 100049, China

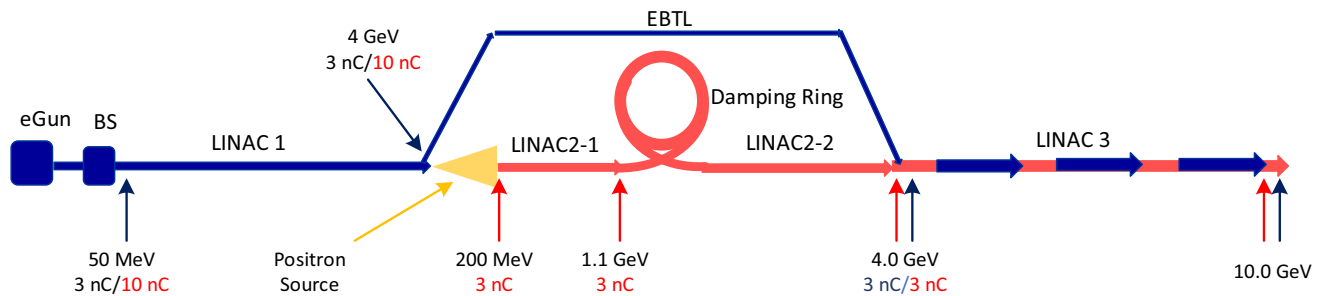


Fig. 1 (Color online) Layout of CEPC injector

accelerating to approximately 200 MeV in the pre-acceleration section. Subsequently, the positron beams are accelerated to 4.0 GeV via two Linac sections, i.e., Linac2-1 and Linac2-2. A damping ring is adopted between Linac2-1 and Linac2-2 to reduce the emittance of the positron beam. The third acceleration section increases the energy of both the electrons and positrons to approximately 10 GeV.

To provide sufficient positrons with reasonable beam quality, a high positron yield and capture efficiency of the positron source are essential. A transverse phase-space matching device is critical for achieving high capture efficiency. Two matching methods are typically used [5–8]. One is the quarter-wave transformer (QWT), where a short solenoid structure is typically employed. The other is an adiabatic matching device (AMD) that uses a magnetic FC. The main difference between these two methods is the energy acceptance. The QWT depends significantly on the beam energy with narrow-band matching. This method is suitable for low-energy positron accelerators. Meanwhile, the AMD has a higher energy acceptance [9, 10].

Similar FCs have been developed at the SLAC National Accelerator Laboratory (SLAC), High Energy Accelerator Research Organization (KEK), and Institute of High Energy Physics (IHEP) [10–13]. However, these FCs cannot achieve a peak magnetic field of 6 T, which is required for the proposed CEPC. Considering the positron beam requirement of the CEPC, an AMD matching system comprising an FC, a pulsed power supply, and an auxiliary equipment is necessitated. This paper introduces the design, development, and preliminary tests of this FC system. Section 2 summarizes the physical design of the positron source. Section 3 introduces the design of the FC and the development of solid-state pulse modulators. Section 4 presents the offline calibration of the magnetic FC based on small signal measurement, test results for the solid-state pulse modulator, and measurements of the online magnetic field. A brief conclusion is presented in Sect. 5.

2 Positron source

The PSPAS is one of the core components of the CEPC Linac and is composed of a conversion target, an FC, a capture section, a pre-accelerating section, and a beam separation system. The layout of the PSPAS is shown in Fig. 2.

A large number of positrons can be produced by an electromagnetic cascade shower when high-energy electrons collide with targets made of high atomic number materials. To obtain a positron beam with a bunch charge exceeding 3 nC, the energy and maximum bunch charge of the incident electron beam were set as 4 GeV and 10 nC, respectively. Based on the simulations, a cylindrical tungsten target with a thickness of 15 mm was adopted. The target was embedded in a cuboid copper block for support and cooling.

Electrons, positrons, and photons with a wide energy spectrum were emitted from the target. The positron beam at the target exit exhibited a small transverse beam size and a high transverse divergence; therefore, it must be collimated sufficiently to obtain a low transverse divergence to match with the subsequent section. To fulfill the required capture, an AMD was inserted between the target and the subsequent acceleration section. The required magnetic field, realized by the FC and solenoids, changed from a peak value of 6 T to a constant 0.5 T. The beam distributions at the exit of the target and AMD are shown in Fig. 3. The main parameters of the positron source are listed in Table 1.

3 FC System

3.1 Magnetic field simulation

The magnetic FC was designed to provide a focusing magnetic field that varies gradually along the z-axis. A 0.5-T uniform field in the acceleration structure was generated by other solenoids and is not discussed herein. The basic structure of the magnetic FC was based on the design of positron

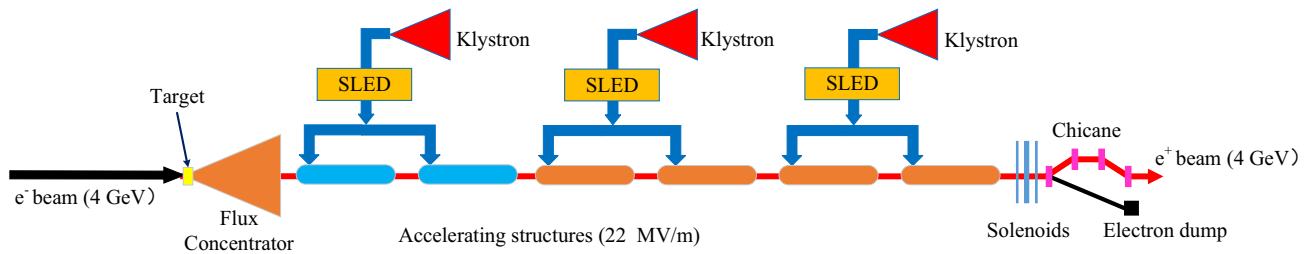


Fig. 2 (Color online) Layout of CEPC PSPAS

Fig. 3 (Color online) Beam distribution at exit of target and AMD

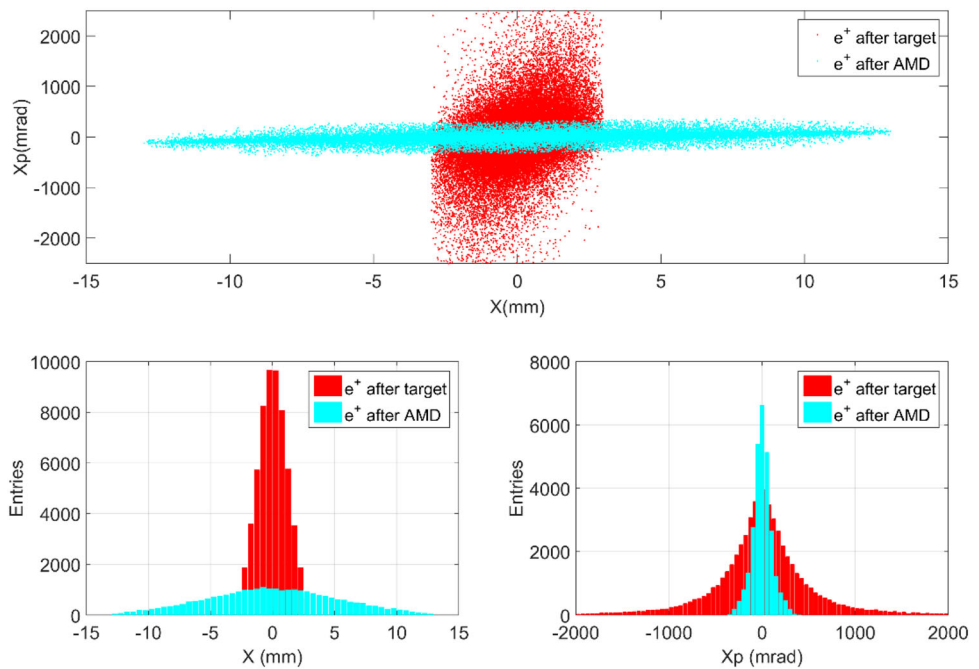


Table 1 Main parameters of proposed CPEC positron source

Parameter	Value
Repetition frequency (Hz)	100
e ⁻ beam energy on target (GeV)	4
e ⁻ bunch charge on target (nC)	10
Norm. RMS. Emittance (e ⁺) (mm·mrad)	2400
e ⁺ beam energy (MeV)	200
e ⁺ bunch charge (nC)	3
e ⁺ beam size@target (mm)	0.5
Deposited power (kW)	0.78
Capture system	AMD
Magnetic field (T)	6→0.5
e ⁺ yield @ CS exit(e ⁺ /e ⁻)	0.55

sources at the SLAC and BEPC. A schematic diagram of the CEPC positron source is shown in Fig. 4a. The trumpet-shaped concentrator comprised a 12-turn copper coil. Every adjacent turn of the coils was separated by a distance of 0.2 mm. The inner diameters of the coils were varied

gradually from 7 to 52 mm, and the outer diameters of the coils were fixed at 106 mm. The total longitudinal length of the concentrator was 100 mm.

The magnetic field of the FC was simulated using Opera with transient TR modules. Because the concentrator exhibited rotational symmetry, a two-dimensional model was used in the simulation. The magnetic field was excited by half-sine current pulses with a peak current of 15 kA, bottom width of 5 μs, and output time of 2.5 μs. The simulation results are presented in Fig. 3. Figure 4b shows the spatial magnetic field density, and Fig. 4c shows the field distribution along the center axis of the FC. As shown in Fig. 4c, the maximum magnetic field on the central axis was 6.3 T, which fulfills the physical design requirement. A three-dimensional model was established using CST 3D EM simulation and analysis software, and the results were verified.

3.2 Mechanical structure and thermal analysis

The mechanical design of the FC is shown in Fig. 5a. The FC was designed to operate at a repetition rate of

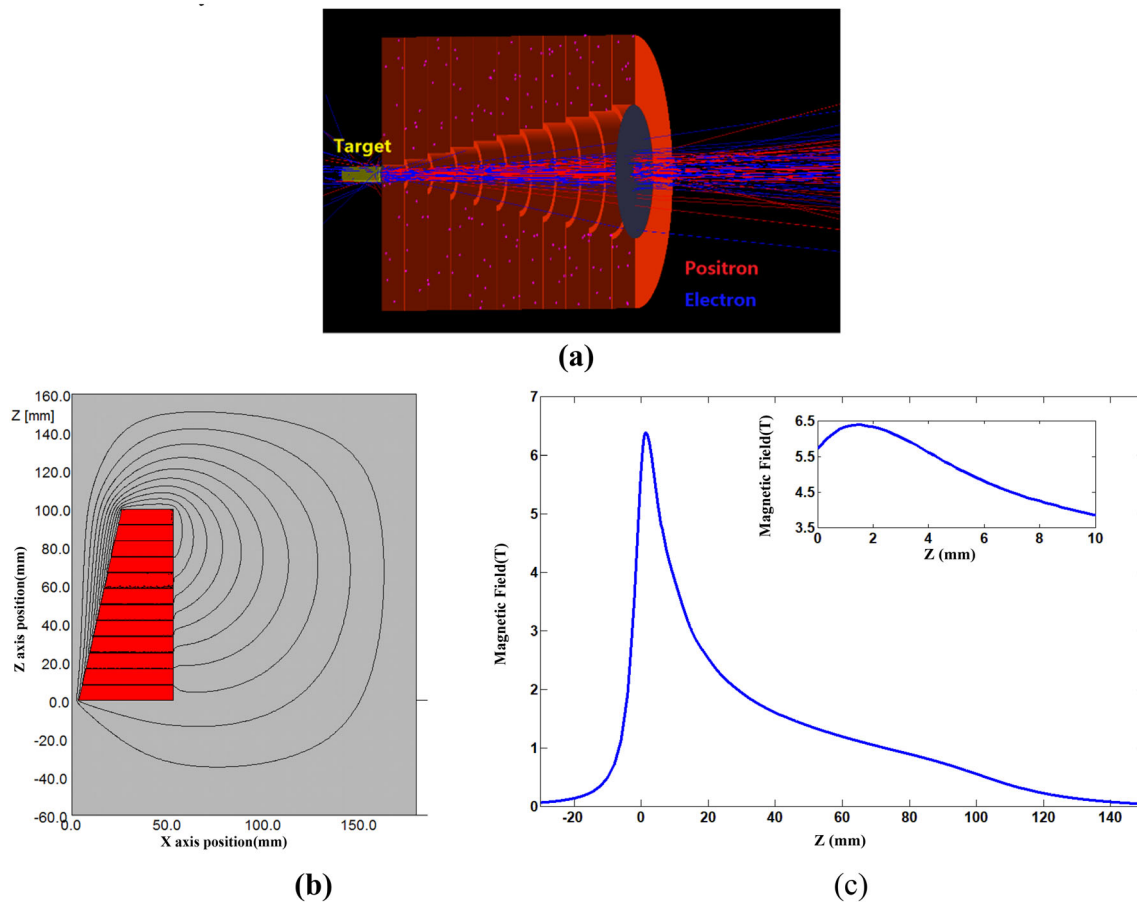


Fig. 4 (Color online) Simulation of magnetic field generation from flux concentrator. **a** Schematic diagram of target and AMD. **b** Magnetic field density. **c** Magnetic field distribution along center axis

50 Hz and a peak current of 15 kA. Heating caused by the exciting current should be considered, and a water-cooling system was adopted. A copper pipe was installed on the outer surface of the magnetic FC coil to allow the cooling water to pass through. The outer and inner diameters of the copper coil measured 5 and 3 mm, respectively. Additionally, this pipe was used to connect cables from the modulator power supply. ANSYS software was used to calculate the temperature and heat distribution using the finite element method. The surface of the FC was set to air commutation, and the ambient and initial water temperatures were set to 20 °C. The water flow rate was 0.5 L/min. The simulated results are presented in Fig. 5b. As shown, the temperature increased to 24.159 °C as cooling water was flowed after the system stabilized. For a short time test with a reduced repetition rate, air cooling might be sufficient. Nonetheless, a water-cooling system is necessitated for normal operations.

During the manufacture of the FC, issues related to high vacuum, high-voltage insulation, radiation resistance, installation, and water cooling were considered. Consequently, a cooperation memorandum of understanding was

signed by the project team and KEK members for the use of the FC spiral cutting technique. Additionally, the manufacturer of the FC has delivered a completed FC to the IHEP for testing. The test results confirmed the reliability and design specifications of the FC. Follow-up experimental research will be conducted in the future.

3.3 Solid-state modulator

A pulse modulator was developed to provide a 15-kA current for the FC. A schematic illustration of the pulse modulator is shown in Fig. 6. The system uses two high-voltage DC power supplies (HVPSs) to charge capacitor C_0 . Each HVPS uses a high-frequency series resonance-type charging power supply, which exhibits constant current charging and short-circuit resistance [14, 15]. The average current per unit is 0.9A. Because the repetition rate of the CEPC positron source is 100 Hz, the charging and discharging units of the modulator are designed to function at a 50 Hz repetition rate. The repetition rate can be increased by adding a parallel charging power supply. When the energy storage capacitor reaches the rated

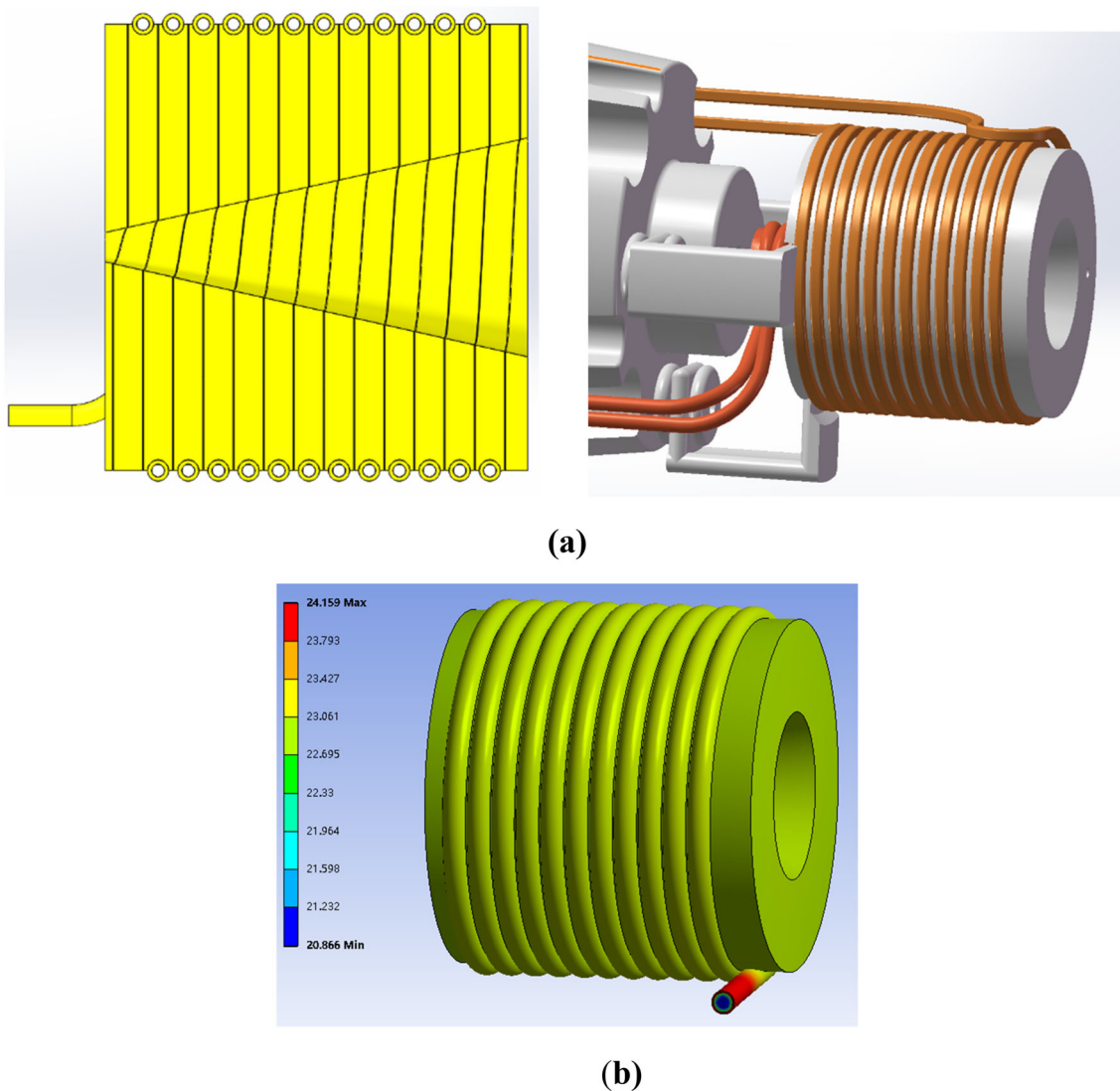


Fig. 5 (Color online) Mechanical structure and water-cooling simulation. **a** Cross section and three-dimensional model of flux concentrator; **b** temperature distribution with water cooling

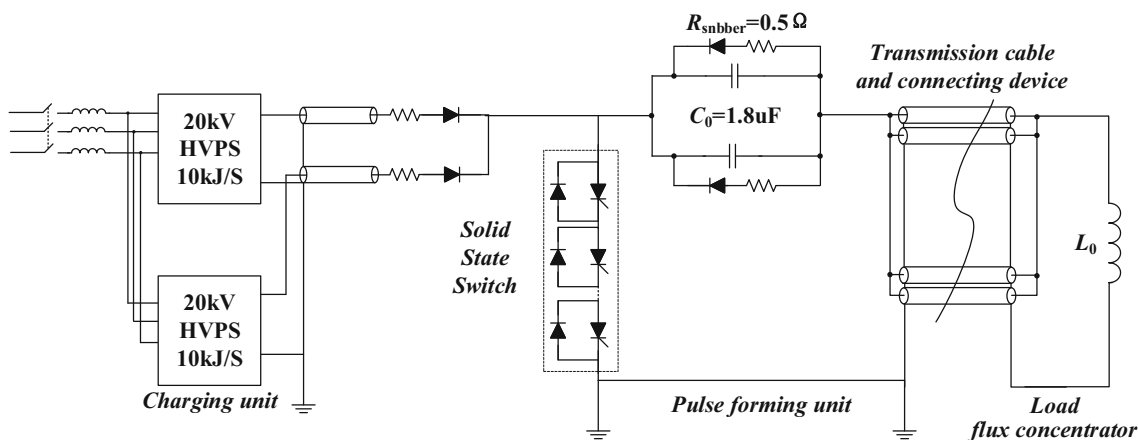


Fig. 6 Schematic illustration of solid-state modulator and output waveform simulation

voltage, the timing signal triggers the discharge switch to turn on, and the required pulsed current is generated in the RLC circuit formed by the energy storage capacitor, load inductance, and equivalent impedance. The design parameters of the magnetic pulse modulator are listed in Table 2.

The all-solid-state switch assembly scheme was adopted instead of the heavy hydrogen thyratron based on the development of high-voltage discharge switches [16–18]. This technique has been reported to exhibit high reliability and a long lifetime [19, 20]. In this study, thyristors were selected as solid-state switches based on tests performed on the IGBT, thyristor solutions, and considerations of the peak current, repetition rate, pulse rising time, and comprehensive cost. The switch assembly was composed of six anti-conduction devices connected in series. The maximum withstand voltage of the assembly was 20 kV. The drive unit was triggered by an optical signal. The compact stacking structure of the switch assembly ensured a low self-inductance. Eight sets of energy storage pulse capacitors, absorption resistors, fast recovery diodes, and transmission cables were symmetrically distributed around the solid-state switch assembly to form a coaxial transmission structure. This compact arrangement can effectively reduce discrete spurious parameters.

Because the load, i.e., the FC, was located in the tunnel, whereas the modulator was in the equipment gallery, a long transmission line was required to connect the load and modulator. To reduce the distributed inductance, twenty 15-m-long cables and specially designed parallel connectors were used to transmit the pulse current. After optimizing the damping circuit, an ideal current pulse can be obtained theoretically.

3.4 Interlock and control system

The FC was installed in a vacuum chamber with a pressure lower than 5×10^{-7} mbar. A sputter ion pump

Table 2 Specifications of pulse power supply

Parameter	Value
Input voltage (V)	$380 \pm 10\%$
Output pulse current (kA)	15
Pulse width (μs)	5
Output waveform (half sine)	
Repeat frequency (Hz)	50
Current stability (%)	$< 0.1\%$
Capacity peak voltage (kV)	15
Energy storage capacitor (μF)	1.8
Equivalent inductance (μH)	0.5
Load inductance (μH)	0.8

and vacuum gauge were employed to achieve and measure such a high vacuum, respectively. During the high-voltage conditioning of the FC, the vacuum pressure can deteriorate by two orders of magnitude. In addition, the temperature of the concentrator can increase owing to continuous heating by the excitation current. Therefore, the vacuum and temperature were interlocked with the modulator. The gate driving signals of solid-state switch assembly were monitored by the control system through optical fibers to ensure the safety of the devices under extreme conditions, such as low-voltage, over-voltage, over-current, gate drive fault, and component failure.

A Yokogawa F3 high-performance PLC unit was used as the main controller. Its digital I/O and analog module can be easily expanded to accommodate the requirement of different multichannel signal processing. The control system was developed based on EPICS [21, 22], and a soft IOC was executed in the PLC to control and monitor the device. The runtime data were shared with other systems through channel access.

4 Bench test

FC Bench tests were performed to verify the performances of the FC and modulator.

4.1 Bench test system

The bench test system includes a solid-state modulator (as described in the previous section), mechanical support system, detection coil, and LeCroy wavepro HD4096 oscilloscope (with a bandwidth of 2.5 GHz and a sampling rate of 20 GS/s). A current transformer (Roche coil CWT150b) was used to measure the pulse current with a transformation ratio of 0.2 mV/A. The pickup coil was composed of five turns of enameled copper wire with a diameter of 0.6 mm and an outer diameter of 3 mm. It was installed inside the FC by docking it with the vacuum flange through a customized adjusting device and then aligned precisely such that it can move along the center axis of the concentrator to enable magnetic field measurements at different longitudinal positions. An oscilloscope was used to record the induced signal of the coil and the output waveform of the modulator. The FC and bench test system are shown in Fig. 7.

4.2 Theoretical Bases of Measurement

The FC operates in the pulse mode, and the magnetic field changes with time. If a coil made of a conducting wire is placed inside the magnetic field, then a varying magnetic flux will occur around the coil. According to Faraday's law

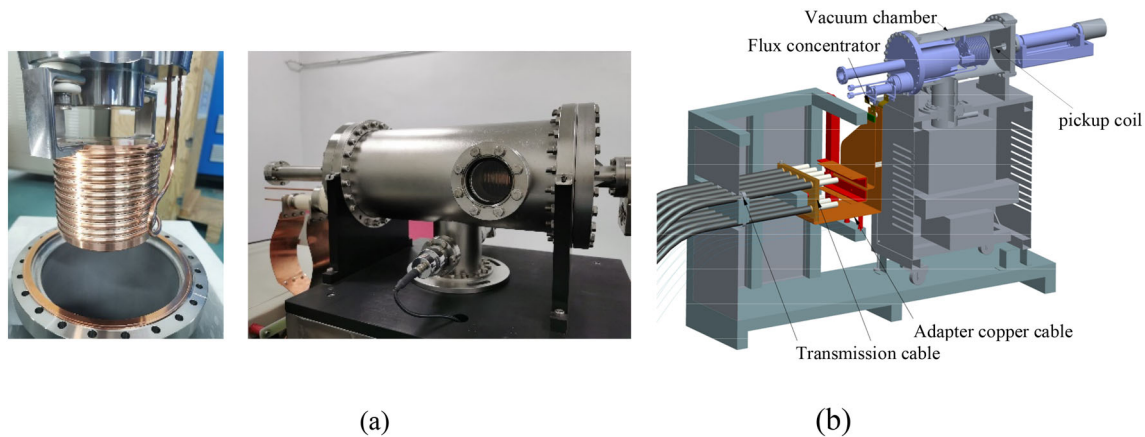


Fig. 7 (Color online) Flux concentrator prototype and measurement device. **a** Flux concentrator prototype; **b** testing device

of electromagnetic induction, an electromotive force is induced owing to a varying magnetic flux. The electromotive force is expressed as

$$\varepsilon = n \frac{d\phi}{dt}, \quad (1)$$

where n is the number of turns in the coil. This electromotive force can be measured in terms of voltage, using an oscilloscope. Equation (1) can be rewritten as.

$$\varepsilon dt = n d\phi \quad (2)$$

Integrating Eq. (2) yields

$$\int_0^{\phi} n d\phi = \int_0^t \varepsilon dt \quad (3)$$

and

$$n\phi = nBS = \int_0^t \varepsilon dt, \quad (4)$$

where S is the coil area. As previously described, the magnetic induction intensity can be calculated using the integrated induced EMF. This can be achieved using the integral function of the oscilloscope. Referring to BEPCII's small signal calibration of the coil and an offline test for the FC, the magnetic fields corresponding to the peaks of 12 and 15 kA were scaled to 5.32 and 6.3 T, respectively.

4.3 Pulse performance of modulator

After a full power conditioning, the modulator yielded a waveform with a peak current of 15.1 kA and a peak voltage of 15.6 kV. The system was operated at a repetition rate of 50 Hz for long-term tests and yielded excellent stability. As shown in Fig. 8, the measured current pulse did exhibit high-frequency ripples, which are typically observed in heavy hydrogen thyratron-based modulators. In terms of the pulse output waveform quality of the solid-

state modulator, compared with the modulators based on a heavy hydrogen thyratron in the BEPCII project [10], the optimized design yielded an almost ideal half-sine pulse output, which resulted in a higher peak current and no high-frequency ripples.

4.4 Magnetic field measurement

The induced electromotive force signal was directly measured using a Teledyne LeCroy oscilloscope, and the current waveform of the modulator output was measured simultaneously. The magnetic induction intensity can be calculated by integrating the induced electric signal and dividing it by the number of turns and area. The magnetic field distribution can be obtained by performing measurements at different axial positions. Figure 9 shows the measured waveforms with a modulator output that peaked at 9.15 kA. As shown in the figure, the measured magnetic field was consistent with the modulator's output in the time domain.

During the experiment, the amplitude of the modulator output increased gradually. The waveforms of the coil signal, modulator output current, and calculated magnetic induction intensity were recorded at several different output levels of the modulator. However, arcing occurred when the peak current exceeded 10 kA, owing to the coil in the vacuum chamber. To ensure safety, the magnetic field was measured with a peak current of 9.15 kA. The magnetic field at higher currents was obtained via linear scaling.

During the measurement, the axial position of the coil was varied in small increments. At each position, the electromotive force signal from the coil and its integral were recorded using an oscilloscope. The magnetic induction intensity was calculated using Eq. (4). In the equation, t is the time when the exciting current reaches its peak value. The calculated field B was plotted as a function

Fig. 8 (Color online) Current output waveforms of modulators

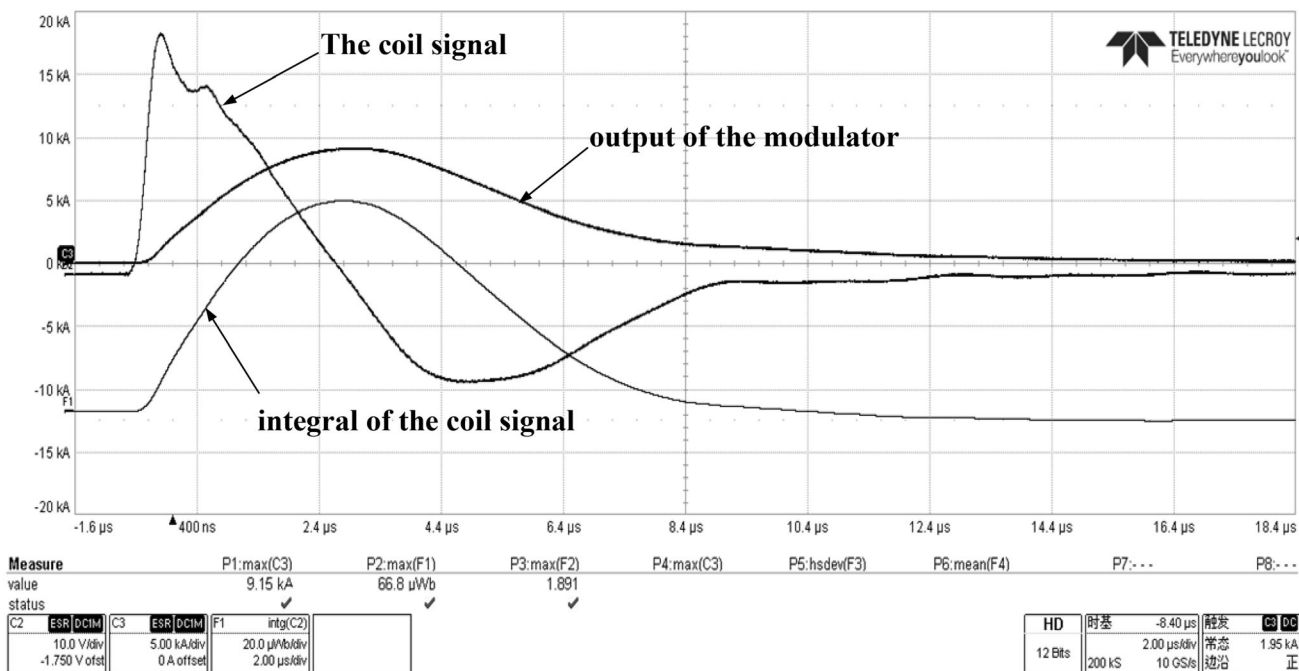
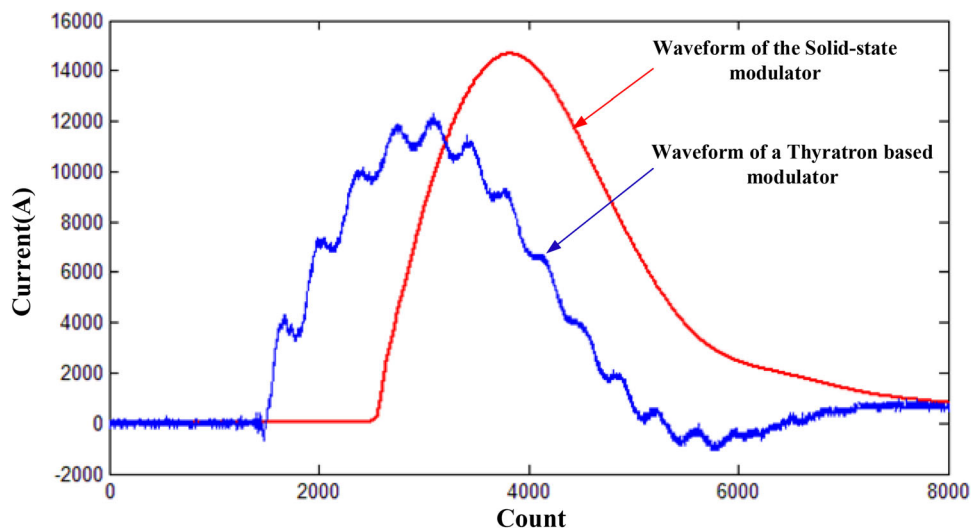


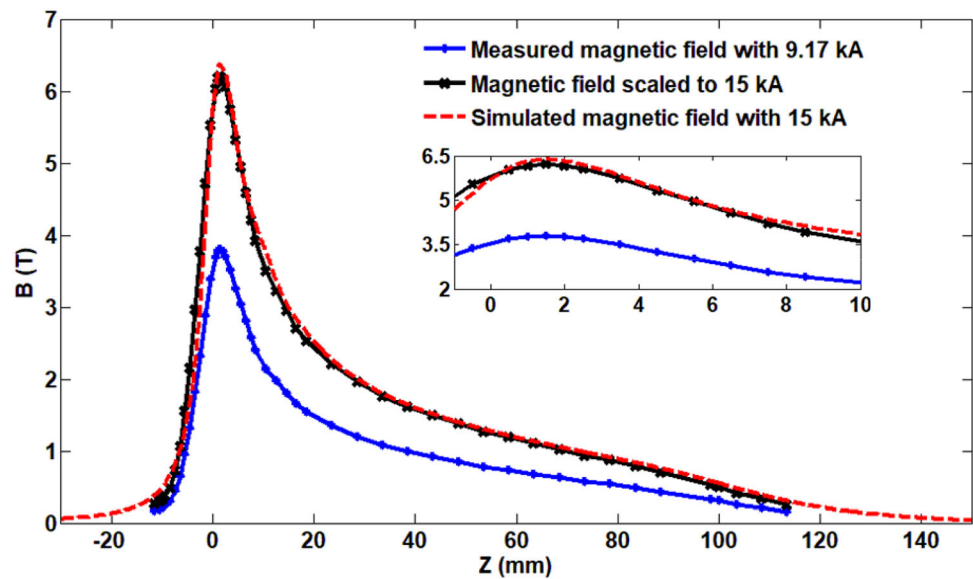
Fig. 9 Measured coil signal and modulator output waveforms. Magnetic induction intensity was integrated from coil signal. Modulator output exhibited peak current of 9.15 kA

of the axial position, as shown in Fig. 10. After scaling this result to that of 15 kA by multiplying with a factor of 15/9.15, the scaled curve was consistent with the simulated one with a peak current of 15 kA, as shown in Fig. 10. These results indicate the following two facts. First, the manufactured FC agreed well with the designed parameters. Second, by supplying the FC, an exciting current with a peak current of 15 kA and a magnetic field of 6.2 T can be obtained.

5 Conclusion

As the key technology of the CEPC positron source, an FC and its solid-state pulsed modulator were developed. A magnetic field with a peak value of 6 T was achieved by supplying a current that peaked at 15 kA. The solid-state modulator produced a current pulse of 15.5 kA with a high voltage of 15.6 kV. An all-solid-state switch was used as the discharge switch. After optimizing the parameters of the switch, a half-sinusoidal pulsed current output was obtained without high-frequency ripples. Subsequently, the peak and distributed magnetic fields were calculated and

Fig. 10 (Color online) Measured and simulated magnetic fields as a function of axial position



scaled. The successful development of the device provides a good technical foundation for the development of CEPC positron sources, as well as a reference for the development of similar devices both domestically and abroad.

Author contributions All authors contributed to the study conception and design. Material preparation, data collection, and analysis were performed by Jing-Dong Liu, Xiao-Ping Li, and Cai Meng. The first draft of the manuscript was written by Jing-dong Liu, and all authors commented on previous versions of the manuscript. All authors read and approved the final manuscript.

References

1. The CEPC-SPPC Study Group, CEPC Conceptual Design Report. IHEP-CEPC-CDR-2018-09. [arXiv: 1809.00285](https://arxiv.org/abs/1809.00285)
2. C. Meng, J.R. Zhang, X.P. Li, CEPC Linac design. *Int. J. Mod. Phys. A* **34**(13n14), 1940005(2019), <https://doi.org/10.1142/S0217751X19400050>
3. H.J. Zheng, J. Gao, J.Y. Zhai, et al., RF design of 650-MHz 2-cell cavity for CEPC. *Nucl. Sci. Tech.* **30**: 155 (2019)
4. C. Meng, X.P. Li, G.X. Pei et al., CEPC positron source design. *Radiat. Detect. Technol. Methods* **3**, 32 (2019). <https://doi.org/10.1007/s41605-019-0110-6>
5. Y.L. Han, C. Bayar, A. Latina et al., Optimization of the CLIC positron source using a start-to-end simulation approach involving multiple simulation codes. *Nucl. Instrum. Methods Phys. Res. A* **928**, 83–88 (2019). <https://doi.org/10.1016/j.nima.2019.03.044>
6. H. Nagoshi, M. Kuribayashi, M. Kuriki et al., A design of an electron driven positron source for the international linear collider. *Nucl. Instrum. Methods Phys. Res. A* **953**, 1–9 (2020). <https://doi.org/10.1016/j.nima.2019.163134>
7. A. Variola, Advanced positron sources. *Nucl. Instrum. Methods Phys. Res. A* **740**, 21–26 (2014). <https://doi.org/10.1016/j.nima.2013.10.051>
8. V. Bharadwaj, Y. Batygin, R. Pitthan, et al. Design Issues for the ILC Positron Source, Proceedings of the IPAC2005, <https://doi.org/10.1109/PAC.2005.1591422>
9. J.T. Liu, Z.Q. Geng, X.J. Sun et al., Development of the BEPCII positron source flux concentrator. *High Energy Phys. Nucl. Phys.* **29**(4), 404–407 (2005)
10. G.X. Pei, Y.L. Sun, J.T. Liu, BEPCII positron source. *High Energy Phys. Nucl. Phys.* **30**(1), 66–70 (2006). https://doi.org/10.1142/9789814401043_0015
11. A.V. Kulikov, S.D. Ecklund. SLC positron source pulsed flux concentrator, 1991 IEEE Particle Accelerator Conference (PAC). <https://doi.org/10.1109/PAC.1991.164851>
12. H.T. Wang, W.M. Liu, W. Gai, Modeling and prototyping of a flux concentrator for positron capture. *IEEE T. Magnetics.* **44**(10), 2402–2408 (2008). <https://doi.org/10.1109/TMAG.2008.2001844>
13. K. Akai, K. Furukawa, H. Koiso et al., SuperKEKB collider. *Nucl. Instrum. Methods Phys. Res. A* **907**, 188–199 (2018). <https://doi.org/10.1016/j.nima.2018.08.017>
14. D.S. Kim, B.K. Lee, S.S. Park et al., High-capacity capacitor charging power supply for a pulse modulator. *J. Korean Phys. Soc.* **76**, 547–550 (2020). <https://doi.org/10.3938/jkps.76.547>
15. S.R. Jang, S.H. Ahn, H.J. Ryoo et al., Novel high voltage capacitor charger for pulsed power modulator. 2010 IEEE International Power Modulator and High Voltage Conference, Atlanta, GA, 317–321(2010) <https://doi.org/10.1109/IPMHVC.2010.5958357>.
16. D. Bortis, J. Biela, J.W. Kolar, Active gate control for current balancing of parallel-connected IGBT modules in solid-state modulators. *IEEE T. Plasma Sci.* **36**(5), 2632–2637 (2008). <https://doi.org/10.1109/TPS.2008.2003971>
17. S.-M. Park, S.-H. Song, H.-B. Jo et al., Solid-state pulsed power modulator for 9.3 GHz 1.7 MW X-band magnetron. *IEEE T. Ind. Electron.* **68**(2), 1148–1154 (2021). <https://doi.org/10.1109/TIE.2020.2967728>
18. U.R. Vemulapati, E. Bianda, D. Torresin et al., A method to extract the accurate junction temperature of an igct during conduction using gate–cathode voltage. *IEEE T. Power Electron.* **31**(8), 5900–5905 (2016). <https://doi.org/10.1109/TPEL.2015.2492621>
19. J. Choi, Y.M. Shin, Y.W. Choi et al., Solid-state pulse modulator for a 17-MW X-band magnetron. *J. Korean Phys. Soc.* **64**, 1267–1271 (2014). <https://doi.org/10.3938/jkps.64.1267>
20. D.A. Komarov, S.P. Maslennikov, Solid-state modulator for high-power microwave devices with grid control. *J. Commun.*

- Technol. Electron. **64**, 64–68 (2019). <https://doi.org/10.1134/S1064226919010091>
21. J.J. Liu, X.P. Ma, G.X. Pei et al., Phase-stabilized RF transmission system based on LLRF controller and optical delay line. Nucl. Sci. Tech. **30**, 177 (2019). <https://doi.org/10.1007/s41365-019-0697-9>
22. W.B. Wu, K. Xuan, W. Xu et al., Development of a control system for the fourth-harmonic cavity of the HLS storage ring. Nucl. Sci. Tech. **29**, 153 (2018). <https://doi.org/10.1007/s41365-018-0497-7>